

PAPER • OPEN ACCESS

Development and validation of a novel fibre-optic respiratory rate sensor (FiRRS) integrated in oxygen delivery devices

To cite this article: R Sinha *et al* 2021 *J. Phys. D: Appl. Phys.* **54** 124002

View the [article online](#) for updates and enhancements.



IOP | ebooks™

Bringing together innovative digital publishing with leading authors from the global scientific community.

Start exploring the collection—download the first chapter of every title for free.

Development and validation of a novel fibre-optic respiratory rate sensor (FiRRS) integrated in oxygen delivery devices

R Sinha^{1,4}, Francisco U Hernandez^{2,4}, C He² , S Korposh² , R Correia² , A M Norris^{1,3}, C Liu², B R Hayes-Gill² and S P Morgan² 

¹ Department of Anaesthetics, Queen's Medical Centre, Nottingham University Hospitals NHS Trust, Nottingham NG7 2UH, United Kingdom

² Optics and Photonics Group, Faculty of Engineering, University of Nottingham, Nottingham NG7 2RD, United Kingdom

³ Department of Anaesthesiology, King Faisal Specialist Hospital and Research Centre, Riyadh, Saudi Arabia

E-mail: steve.morgan@nottingham.ac.uk

Received 11 August 2020, revised 18 November 2020

Accepted for publication 3 December 2020

Published 14 January 2021



CrossMark

Abstract

Respiratory rate (RR) monitoring provides crucial information on the overall health condition of patients and a reliable, low cost RR monitor for normal hospital inpatient or home use would be of significant benefit. The proposed system measures light reflection from a Fibre Bragg Grating (FBG) located near, and the total reflection spectrum from a humidity sensing film deposited at, the tip of an optical fibre. Every breath causes a shift in the wavelength reflected from the FBG and intensity change in the overall reflection spectrum. The accuracy of different techniques is investigated in a two-part study with 15 healthy volunteers. In part 1, the participants' respiration rate followed a handheld mobile application at 5, 12 and 30 breaths per minute with simultaneous measurement using the optical fibre system, thoracic impedance pneumography (TIP) and capnometry device (where possible). Two types of medical face masks and a nasal cannula with oxygen delivery rates were investigated. In part 2, participants wore an anaesthetic face mask and breathed at normal and low tidal volumes to evaluate whether low tidal volumes could be detected. The most accurate measurement of RR was through monitoring the Bragg wavelength shift (mean accuracy = 88.1%), followed by the intensity change at the Bragg wavelength (mean accuracy = 78.9%), capnometry (mean accuracy = 77.8%), area under the overall spectrum (mean accuracy = 65.4%) and TIP (mean accuracy = 43.1%). The Fibre-optic Respiratory Rate Sensor system (FiRRS) can differentiate between normal and low tidal volumes (p -value < 0.05) and demonstrated higher accuracy than capnometry measurement of end-tidal carbon dioxide in exhaled air. These latter two monitors measured RR more accurately

⁴ These authors contributed equally to this research.



Original content from this work may be used under the terms of the [Creative Commons Attribution 4.0 licence](https://creativecommons.org/licenses/by/4.0/). Any further distribution of this work must maintain attribution to the author(s) and the title of the work, journal citation and DOI.

than TIP. A comparable accuracy in the measurement of RR was obtained when the **FIRRS** was implemented in nasal cannula and face masks.

Supplementary material for this article is available [online](#)

Keywords: optical fibre sensor, fibre Bragg grating (FBG), respiratory rate (RR), medical face mask

(Some figures may appear in colour only in the online journal)

1. Introduction

Previous research has demonstrated that there is a significant incidence of respiratory failure (3.4%) in patients following surgical procedures under epidural, general and spinal anaesthetics [1]. Apnoeic events are a feature of obstructive sleep apnoea (OSA) which, with increasing prevalence of obesity, is a common problem in surgical patients. Obesity is one of the most important contributory factors in OSA and these patients are at a higher risk of a variety of postoperative complications including apnoeas [2]. It is estimated that 5%–10% of the population may have undiagnosed OSA [3, 4].

Monitoring of vital signs is therefore an important part of safe clinical care in many contexts and particularly in the postoperative setting. At present, a variety of monitors of heart rate, blood pressure and oxygen saturation are in common use, however, respiratory rate (RR) monitoring has proved to be more challenging [5]. There are various respiratory monitoring devices employing differing technologies in use, including haemoglobin saturation (using pulse oximetry) [6] and thoracic impedance pneumography (TIP) via electrocardiogram (ECG) electrodes [7]. Measurement of end-tidal carbon dioxide in exhaled air (capnometry, EtCO₂) can also be used but this is less common outside of anaesthesia and intensive care. Clinical measurement is still frequently carried out by intermittent manual counting of chest wall movement; however, research and developments of RR measurement approaches have been recently classified into three modalities [5]: (a) RR from other physiological signals such as in pulse oximetry or TIP [6, 7]; (b) RR measurement based on respiratory movements such as with accelerometers and gyroscopes recordings [8], with application of either piezoresistive/piezoelectric elements [9, 10] or Fibre Bragg Grating (FBG) sensor array [11] attached to fabrics; (c) RR measurement based on airflow such as with technologies based on hygroscopic sensors [12] and where EtCO₂ capnometry has been established as one of the clinical standards for RR monitoring [13, 14].

There are drawbacks associated with current approaches in the clinical setting. Pulse oximetry is a means to assess gas exchange occurring in the lungs, but it is a poor monitor of ventilation. In particular, there is a delay in identifying hypoventilation or apnoea when subjects are breathing supplemental oxygen, such that the oxygen saturations (SpO₂) may be maintained in the face of significant hypoventilation and even apnoea. Pulse oximetry can also be erroneous due to various factors including displacement, movement artefact and

ambient light [15]. TIP measures electrical impedance changes associated with movement of the chest wall, thoracic volume and blood volume changes with respiration. It can be affected by ECG electrode displacement, motion artefact as well as coughing and sneezing leading to inaccuracies. In the context of increasing obesity, the inability to distinguish obstructive apnoea where there is chest wall movement but no flow of air across the airways has also been noted [14]. Measurement of EtCO₂ in exhaled air is widely used as a ventilatory monitor during anaesthesia, some procedures carried out under sedation and also in some post-anaesthetic and intensive care units. It is an accurate and reliable ventilation monitor in ‘closed’ systems such as those used in anaesthesia and intensive care but is less useful where ‘open’ breathing systems are used and outside of the operating theatre setting. The EtCO₂ analysing unit nevertheless is relatively bulky and expensive. Devices that rely on capnometry such as the Capnomask[®] have been developed and have been demonstrated as being useful in specific situations [14, 16]. However, with increasing flows of oxygen, there is an alteration of the levels of exhaled CO₂ which could give rise to measurement error [14] and each mask requires its own analysing device. Compliance with position of the mask and the cost of the analysing unit are further barriers to wide uptake.

An example of a respiration rate monitor in current clinical practice is the respiR8[®] [13]. This measures RR via an electrical humidity sensor situated in an oxygen mask. It has been noted however [13], that two factors limit the performance of respiR8: (a) low expiratory flow rates and (b) water condensation on the sensor due to lack of drying ambient air flowing over the sensor. These can cause inadequate readings in humidity between inhalation and exhalation that triggers an alarm indicating that ventilation of the patient is insufficient due to low or high RR or inadequate tidal volume. To our knowledge, measuring of RR via humidity in low flow oxygen devices such as nasal cannulas has not been investigated.

As described above the devices in common use for the measurement of RR have significant shortcomings. We have previously reported an optical device which measures humidity in exhaled air on a breath to breath basis, demonstrated in a bench-top model with a ventilator and a lung performance analyser [17]. It uses optical fibre technology that can be easily integrated into oxygen delivery devices such as masks and nasal cannula. Optical fibres are light weight, carry no electrical current, are inexpensive and have demonstrated rapid response time [18, 19]. In addition to humidity sensing, the

probe described in this paper also includes a highly sensitive optical fibre temperature sensor.

Our primary objective was to assess accuracy and reliability of our optical fibre device as a RR monitor (Fibre-optic Respiratory Rate Sensor—FiRRS) using three different types of oxygen delivery devices and to compare it against the current reference standard (EtCO₂ analysis) and manual counting. The main sensing probe consists of a FBG inscribed near the tip of the optical fibre for temperature sensing and a hygroscopic film deposited at the tip of the fibre for humidity sensing. Both temperature and humidity provide the capability to measure RR. Our secondary objectives were (a) to demonstrate statistically the sensitivity of our device in distinguishing between normal and low tidal volumes of respiration, and (b) to collect additional information pertaining to the technical performance of the device and the need for modification.

2. Materials and methods

2.1. Materials

Poly(allylamine hydrochloride) (PAH, MW:~58 000), Sodium Hydroxide (NaOH), Potassium Hydroxide (KOH), and ethanol were purchased from Sigma-Aldrich, U.K. Silica nanoparticles (SiO₂, SNOWTEX 20L, diameter 40–50 nm) were obtained from Nissan Chemical, Japan. All these reagents were of analytical grade and used without further purification. Deionised water (DI water), having resistivity of 18.2 MΩ cm, was obtained from a water purification system (PURELAB Option S/R, ELGA). The optical fibres were boron and germanium co-doped photosensitive fibre (PS1250, Fibercore) to enable FBG inscription.

2.2. Sensing probe fabrication

A thin film composed of nine bilayers of PAH/SiO₂ NPs was coated on the 90° cleaved tip of the optical fibre using the Layer-by-Layer self-assembly method [20, 21]. The implementation of this method on the tip of optical fibres has been previously characterised [17, 22]. In these papers we demonstrated how the number of bilayers impacts the total reflection from the tip (up to 23 bilayers) and it has been found that an optimum sensitivity lies between 9 and 11 bilayers of PAH/SiO₂ NPs [22, 23]. The Layer-by-Layer method followed these steps: (a) treatment of the cleaved surface-tip with 1 wt% of KOH in ethanolic solution (ethanol:H₂O, 3:2 v v⁻¹) for 20 min to hydroxylate the fibre surface; (b) wash with deionized water and dry with nitrogen, followed by immersion of the fibre tip in 0.17 wt% of positively charged polymer PAH solution (pH: 10–11) for 15 min; (c) wash and dry, and immerse the fibre tip into a solution containing negatively charged SiO₂ NPs for 15 min; (d) after deposition of the SiO₂ NPs, wash and dry and repeat steps (b) and (c) until the desirable number of bilayers of (PAH/SiO₂ NPs)_x is created, where x is the number of bilayers. The coated optical fibre was dried at room temperature in the laboratory for 24 h before use.

FBGs were fabricated using a frequency quadrupled Nd:YAG UV laser emitting at a wavelength $\lambda = 266$ nm

(Photonic Solutions Ltd, Continuum minilite I, repetition rate of 10 Hz, output energy 2 mJ at $\lambda = 266$ nm, pulse width 3–5 ns). The phase-mask inscription technique used has been published previously [18, 24] and is implemented through a Talbot interferometer with two highly reflective mirrors (NB1-K04 with Nd:YAG coating, high reflection range 262–266 nm, diameter 1", Thorlabs, Inc.) in the optical set-up. The length of the FBGs fabricated were 3 mm with Bragg wavelengths of 1539 nm and 1555 nm.

2.3. Sensing principle

Respiration can be detected via changes in temperature or relative humidity. The sensing mechanism of an FBG to temperature is widely known to originate from a change in the effective refractive index η_{eff} and the grating period Λ ($\lambda_{\text{Bragg}} = 2\eta_{\text{eff}}\Lambda$) due to temperature change [25, 26]. A shift of the Bragg wavelength (λ_{Bragg}) to higher values is derived from heating the grating and a shift to lower wavelength values from cooling [26]. The humidity sensing mechanism at the tip of the fibre arises from the hygroscopic properties of the multilayer film made of PAH/SiO₂ NPs which behaves as a Fabry-Pérot reflection cavity [18]. On exposure of the hydrophilic film to a humid environment (the tip of the needle of figure 1), water vapour enters the film changing its optical thickness (physical thickness and refractive index) through adsorption and absorption, thus inducing a change in reflectivity [17, 18, 27] across the whole reflected spectrum. The effective refractive index of the PAH/SiO₂ NPs is approximately 1.22 and the intensity changes linearly with % of relative humidity change (% RH) [17]. As the FBGs are fabricated in the same fibre as the humidity sensing tip (section 2.4) the FBG intensities are also affected by the tip reflectivity. This does not affect tracking of the wavelength of shift of the FBG as the reflectance from the tip is much lower (typically 7% of the peak value) than the FBG reflectivity. However, fluctuation in the FBG intensity is also investigated as sensor parameter alongside wavelength shift and overall tip reflectance.

2.4. Optical fibre sensing apparatus

Figure 1 shows the system including the sensing probe containing FBG1 (Bragg wavelength λ_{FBG1} , ca.1539 nm) and a humidity sensing film with nine bilayers (PAH/SiO₂ NPs)₉ at the tip of the fibre, both enclosed within a 21 gauge hypodermic needle (40 mm length and 0.9 mm inner diameter, previously flattened-polished at the tip) to avoid bending and motion artefacts. The system also comprises a Superluminescent Diode (SLD) (Superlum, SLD-761-HP, UK) as a light source with central wavelength 1550 nm and a spectral bandwidth of 45 nm. Light from the SLD travels through an optical circulator (Thorlabs Inc., 6015-3-APC, 1525–1610 nm, USA) towards the single mode fibre having FBG2 (ca. $\lambda_{\text{FBG2}} = 1555$ nm) located 2 m apart from FBG1 and a reflective film that is sensitive to humidity at the tip [17]. The light reflected from the sensor includes the reflectivity from the sensitive film along with the Bragg reflections from

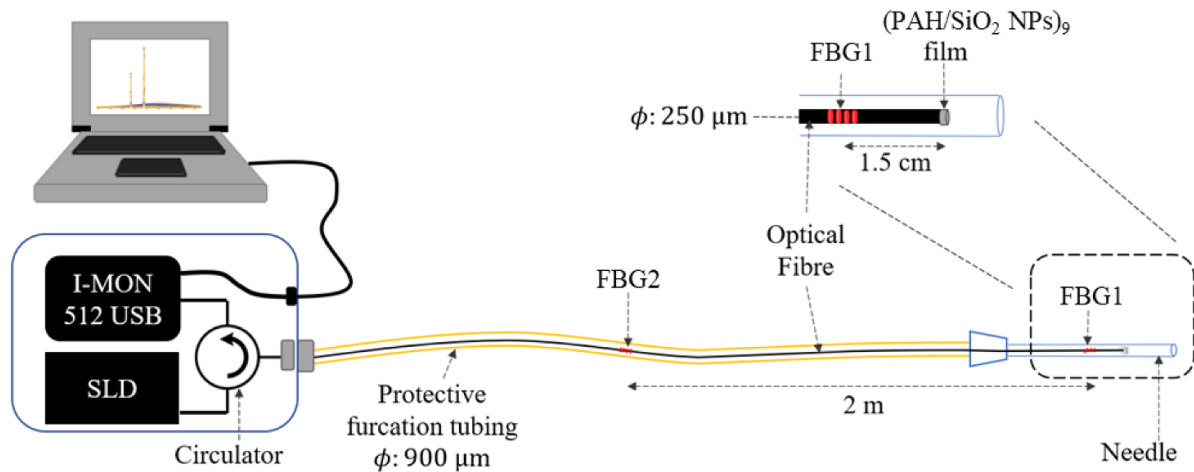


Figure 1. Overall FiRRS sensing system containing a laser diode (SLD), spectrometer (I-MON 512USB), optical circulator, recording laptop and fibre optic respiratory rate sensor enclosed within a 21 gauge hypodermic needle polished at the tip. The box encasing the spectrometer and SLD has dimensions of 20 cm × 25 cm × 12 cm (W × L × H).

FBG1 and FBG2 and is conveyed to a spectrometer (Ibsen Photonics A/S, I-MON 512USB, Denmark) via the optical circulator. The total reflection spectrum is recorded on a computer. Only FBG1 is sensitive to temperature change near the tip of the needle due to respiration. FBG2 was included as a precaution as a reference for room temperature or possible compensation of motion artefacts but was not ultimately required in this study. It is only included in the description to avoid confusion as results presenting the spectrum show two FBG peaks.

2.5. Volunteer study

Ethical approval was obtained from the Research Ethics Committee for the Faculty of Medicine and Health Sciences at the University of Nottingham. This was a single centre study in which healthy volunteers were invited to participate. Following assessment for inclusion and exclusion criteria written consent was obtained. Basic demographic data were collected, and the study was conducted in accordance with good clinical practice [28]. The inclusion criteria considered that participants were healthy adults between 18 and 55 years of age and that they were able to consent and comply with the process. Participants were excluded for one or more of the following reasons (a) inability to understand the purpose of the study or what was involved; (b) inability to provide consent; (c) pregnancy; (d) abnormal upper airway anatomy; (e) any known chronic illness affecting activities of daily living; (f) ongoing respiratory disease. A total of 20 participants were recruited (14 or 15 participants provided usable data due to data acquisition failure in either commercial or FiRRS system but unrelated to sensor performance). 18 participants met the inclusion criteria and had the following characteristics: Median Age = 28 (25–55) years of age, Female participants = 6, Average body mass index (BMI) = 23.77 kg m⁻² and all had normal resting values of heart rate, blood pressure and oxygen saturation recorded before performing the RR study. The basic demographic data of the participants considered within

the inclusion criteria are presented in table S1 (available online at stacks.iop.org/JPD/54/124002/mmedia) in the appendix.

2.5.1. Part 1: accuracy of the device as RR monitor using three different types of oxygen delivery devices. The sensing probe (needle figure 1) was integrated into the oxygen delivery devices being studied (figure 2). Flow rates were based on British Thoracic Society guidelines [29] and found to be comfortable for participants involved in the study. The devices used were:

- Oxygen mask allowing side-stream measurement of end-tidal CO₂—EtCO₂—(Sentri Ecolite™ CO₂ mask, Intersurgical, UK, figure 2(a)) with the oxygen flow rate set to 5 l per minute.
- Nasal cannula (Flexicare Medical Ltd, UK, figure 2(b)) with oxygen flow set at 2–4 l per minute.
- Non-rebreathe mask (Flexicare Medical Ltd, UK, figure 2(c)) with the oxygen flow rate set to 15 l per minute.

Baseline monitoring was established on all participants (ECG, TIP, oxygen saturation). Participants were allowed time to get accustomed to each oxygen delivery device and RR being studied. They synchronised their RR with a handheld mobile application (Paced breathing, T Rex LLC) at 5, 12 or 30 breaths per minute (bpm) according to randomisation sequence. RR measurements were made by: manual counting; the FiRRS system; TIP; and end-tidal CO₂ (where possible). These were conducted with a nasal cannula; oxygen mask with side-stream measurement of EtCO₂; and non-rebreathe masks at the above flow rates for two minutes for every RR studied.

2.5.2. Part 2: measurement of low tidal volumes. After completing part 1 of the study, participants were asked to breathe air via an anaesthetic face mask (figure 3, Economy anaesthetic face mask 1 515 000, Intersurgical Ltd, UK, with FiRRS probe attached) through a closed anaesthetic circuit (Uniflow™

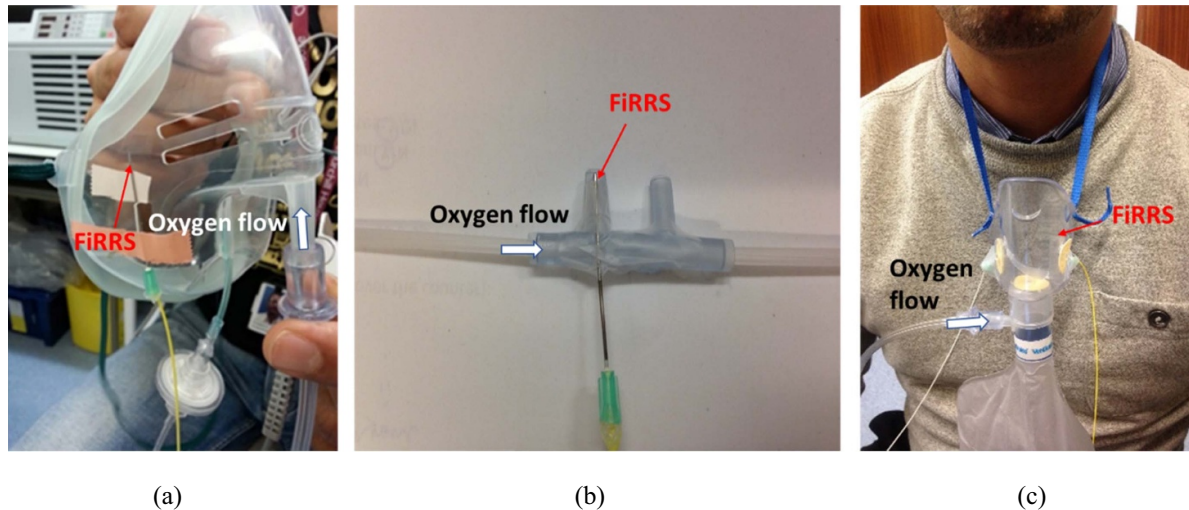


Figure 2. Integration of the sensing probe into (a) CO₂ mask (with EtCO₂ capnometry), (b) nasal cannula and (c) non-rebreather trauma mask.



Figure 3. Anaesthetic mask with needle containing optical fibre inserted and used in part 2 of this research work.

coaxial breathing system, Intersurgical Ltd, UK) using an anaesthetic machine (Aestiva 5, Datex Ohmeda, GE Healthcare, UK) attached to a CO₂ absorber using soda lime (Spherasorb, Intersurgical Ltd, UK) with integrated end-tidal CO₂ monitoring (TramTrac, GE Healthcare, UK). The anaesthetic machine contains an accurate pneumotachograph which displays breath to breath measurement of expired volumes and enabled assessment of the capability of FiRRS to identify low tidal volumes. After allowing a period of time for familiarisation (1 min recording), participants were asked to drop their tidal volumes to under 100 ml for at least 20 breaths. Subjects were then asked to breathe normally again (1 min approximately). Although the devices could be used independently, measurements were only recorded with the FiRRS system while the participants followed the display screen of the anaesthetic machine.

2.6. Signal post-processing for FiRRS and statistical analysis

The spectrometer's LabVIEW software was modified to record raw spectral data and both wavelengths and peak

intensities of the FBGs. All the spectra recorded from the first seven participants were acquired at a sampling frequency of 1 Hz and for the remaining participants it was acquired at 10 Hz. 1 Hz is at the Nyquist sampling frequency for RR = 30 bpm but it was observed during the study that significantly improved signal quality was achieved with 10 Hz. As described in the previous section and after acquisition of data from both parts of the study (RR being recorded for 2–3 min), three parameters were considered for post-processing analysis, the wavelength and intensity of FBG1 and the intensity area under the spectrum between 1529 nm and 1581 nm. The wavelength of FBG1 indicates the temperature whereas the FBG1 intensity and area under the spectrum is affected by humidity at the fibre tip.

2.6.1. Signal post-processing and statistical analysis of part 1.

The data from FBG1 (wavelength FBG1, intensity FBG1) were post-processed using *MATLAB R2020a* using the following procedure: (a) offset baseline calculation using a polynomial fit—*polyfit*—of degree 5; (b) subtraction of the baseline to zero offset; (c) calculation of the Fast Fourier Transform (FFT) of the overall 2–3 min signal after baseline subtraction and (d) detection of the maximum peak of the FFT within the range between 4 bpm and 31 bpm. Data from the area under the spectrum between 1529 nm and 1581 nm was post-processed using the following steps: (e) calculation of the area value for each spectrum recorded during the 2–3 min recording and converting into a trace of change of area over time; (f) subtraction of the mean value calculated from the overall trace of area values for the total 2–3 min recording and calculation of the FFT; (g) detection of the peak of the FFT within the range between 4 bpm and 31 bpm.

Collection of data consisted of the breathing rate measured with the FiRRS system (RR values obtained through FFT and post-processing analysis), the TIP device and the EtCO₂ capnometry device, all recorded from all participants when using the different types of oxygen delivery masks

investigated. The RR values from all devices and participants were gathered into tables and the accuracy of every system was calculated based on the expected value, i.e. the number of successes measured (correct RR values when compared to manual counting) divided by the total of experiments performed with all participants was collected as a relative percentage accuracy.

2.6.2. Signal post-processing and statistical analysis of part 2. The data from FBG1 were processed following part 1 signal processing steps (a) and (b). Step (c) involved calculation of the absolute difference between the maximum peak and minimum trough from the FiRRS response measured for three time intervals: the first minute of recording (normal tidal breathing volume), the second minute (low tidal breathing volume) and the third minute (return to normal tidal breathing volume).

Area under the spectrum data was also processed following step (e) of part 1. This was then followed by (f) subtraction of the mean value calculated from the overall trace of area values for the total recording; (g) calculation of the absolute difference between the maximum peak and minimum trough from the FiRRS response measured for three time intervals: the first minute of recording (normal tidal breathing volume), the second minute (low tidal breathing volume) and the third minute (return to normal tidal breathing volume).

Statistical analysis for this part was completed using the software IBM® SPSS® Statistics 22. Kolmogorov–Smirnov test was used to demonstrate that the acquired data (differences between maximum peak and minimum trough) from the first, second and third minute of recording had normal distribution. A Student's *t*-test was performed between sets of data to investigate whether there was significant difference between normal and low tidal volume of respiration.

3. Results

3.1. Part 1 study: signal acquisition and post-processing analysis example

Figure 4 shows a typical reflection spectrum recorded by the spectrometer during every RR study. The narrow FBG peaks of the measurement FBG1 and reference FBG2 can be clearly observed along with a broader background signal reflected from the fibre tip. The wavelength and intensity of FBG1, and the area under the spectrum between 1529 nm and 1581 nm can be used to monitor RR. Figure 5 presents an example of the measurands obtained from a participant using the Senti Ecolite™ CO₂ mask and following the mobile application at 5 bpm. Figure 5(a) plots the wavelength shift of FBG1 with its baseline removed and its associated FFT is shown in figure 5(b). Figure 5(c) plots the intensity change of FBG1 with its baseline removed and its associated FFT is shown in figure 5(d). Figures 5(e) and (f) show the area under the spectrum and the FFT respectively.

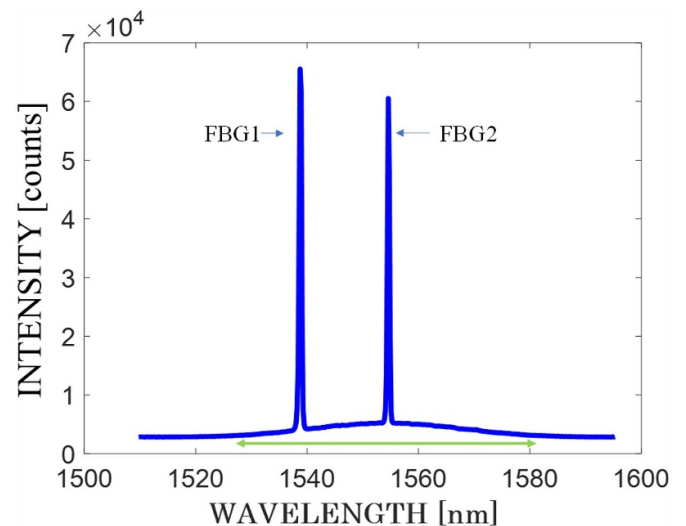


Figure 4. Typical reflection spectrum acquired by the spectrometer (figure 1) at 10 Hz and recorded during every RR study. The measurement FBG1 is centred at ca. 1539 nm and the area under the spectrum considered for analysis was between 1529 nm and 1581 nm (indicated with a green arrow).

3.2. Part 1 study: analysis of whole dataset

Table 1 presents all the RR values measured with manual counting, the FiRRS system, the TIP device and the EtCO₂ capnometry device, all recorded from 15 participants using the Senti Ecolite™ CO₂ mask. Correct RR values measured with the commercial devices and the FiRRS system calculated with the post-processed analysis explained in section 2.5 highlighted in green.

Similar comparison tables of the RR values with the FiRRS system and commercial devices were created for the nasal cannula (2 and 4 l min⁻¹) and non-rebreathe trauma mask (15 l min⁻¹) (supplementary data).

Figure 6(a) provides a graphical summary of all tabulated data from tables 1 and S2–S4 as a bar chart. The accuracy shown in figure 6 refers to the closeness of the measured RR values to manual counting (MC). Each parameter of the FiRRS system (i.e. area under the spectrum, $ws1$ = wavelength shift FBG1, $i1$ = intensity change FBG1) is compared with commercial devices (TIP and EtCO₂) for different breathing devices (CO₂ mask—red bar, trauma mask—blue bar, nasal cannula (low flow)—dark green, nasal cannula (high flow)—light green). It should be noted that EtCO₂ can only be used within masks hence only two values are shown. The most accurate measurement is obtained from the wavelength shift of FBG1 ($ws1$) representing temperature changes of the breath. Similar performance is obtained from EtCO₂ and the intensity of FBG1 ($i1$) representing humidity changes of the breath. TIP provides the least accurate measurement in this study for all oxygen delivery devices. Figure 6(b) demonstrates the accuracy data distribution within a box plot calculated from the values presented in figure 6(a).

Table 1. RR values measured from 15 participants using a Sentri Ecolite™ CO₂ mask (5 l min⁻¹) and showing a comparison between the parameters of the FIRRS system, the TIP device and EtCO₂ capnometry. MC = manual counting (confirmed by observation), RR-area = RR values of the area, RR-ws1 = RR values of wavelength shift of FBG1 and RR-ij = RR values of the intensity change of FBG1.

	MC	RR-area	RR-ws1	RR-ij	TIP	EtCO ₂	MC	RR-area	RR-ws1	RR-ij	TIP	EtCO ₂	MC	RR-area	RR-ws1	RR-ij	TIP	EtCO ₂	
P1	5	5	5	5	13	5	5	5	5	5	13	5	5	5	5	5	13	5	5
	12	12	6	5	12	12	12	12	12	12	12	12	12	12	12	12	12	12	11
	30	30	30	7	30	30	30	30	30	30	31	30	30	30	30	30	30	30	29
P4	5	5	5	5	17	5	5	5	5	10	10	5	5	5	5	5	10	5	5
	12	12	12	12	12	12	12	12	12	12	12	11	12	12	12	12	17	12	12
	30	30	30	30	30	30	30	30	30	29	29	30	30	30	30	29	29	30	30
P5	5	12	5	5	7	5	5	5	5	11	11	12	12	12	12	12	12	12	11
	12	24	30	28	12	12	12	12	12	30	30	29	12	12	12	12	12	12	11
	30	15	30	30	30	30	30	30	30	10	30	29	30	30	30	30	30	30	29
P6	5	14	5	5	20	5	5	5	5	7	7	5	5	5	8	5	10	5	5
	12	10	12	12	16	11	12	12	12	12	12	12	12	12	7	4	12	12	12
	30	20	30	3	31	30	30	30	30	30	30	29	30	30	30	30	30	30	30
P7	5	23	5	5	11	5	5	5	5	19	19	5	5	5	5	10	5	5	5
	12	20	12	12	24	12	12	12	12	14	14	12	12	12	12	12	16	12	12
	30	12	30	30	31	30	30	30	30	30	30	29	30	5	30	30	30	30	30

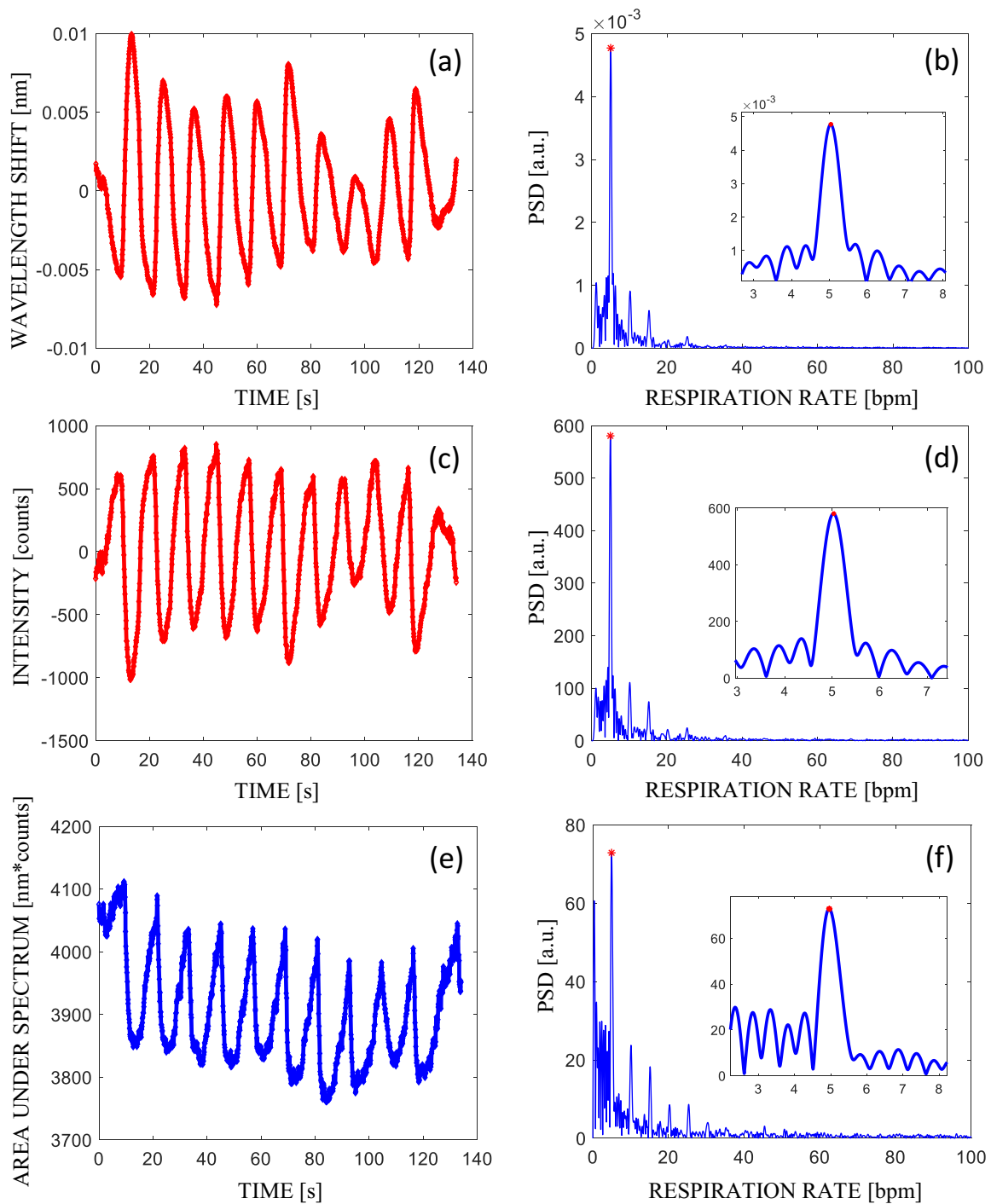
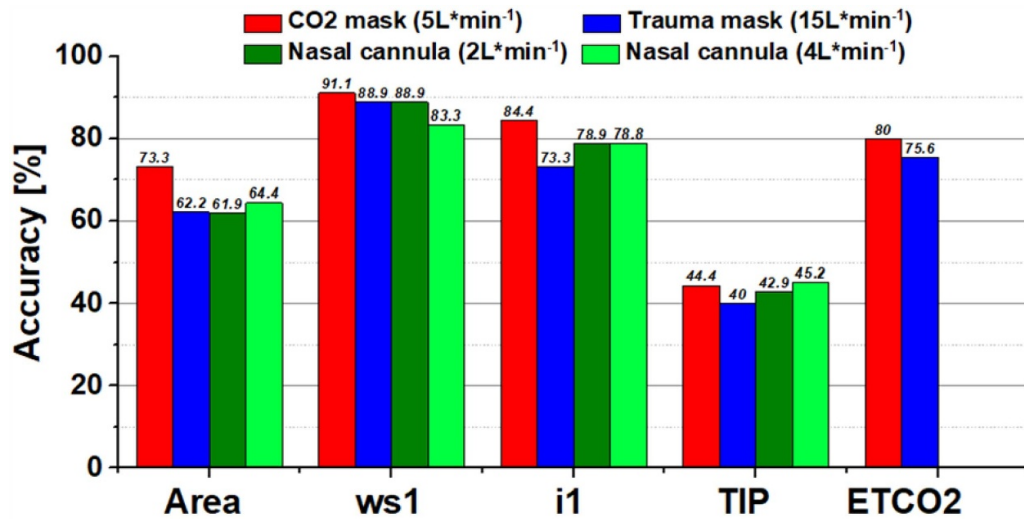


Figure 5. Measurements obtained from a participant using the Senti Ecolite™ CO₂ mask and breathing at 5 bpm. (a) FBG1 wavelength shift with offset baseline subtraction; (b) FFT of (a); (c) FBG1 intensity change with offset baseline subtraction; (d) FFT of (c); (e) area under the spectrum; (f) FFT of (e). PSD = power spectral density and the asterisks show the maximum values calculated through the FFT plots.

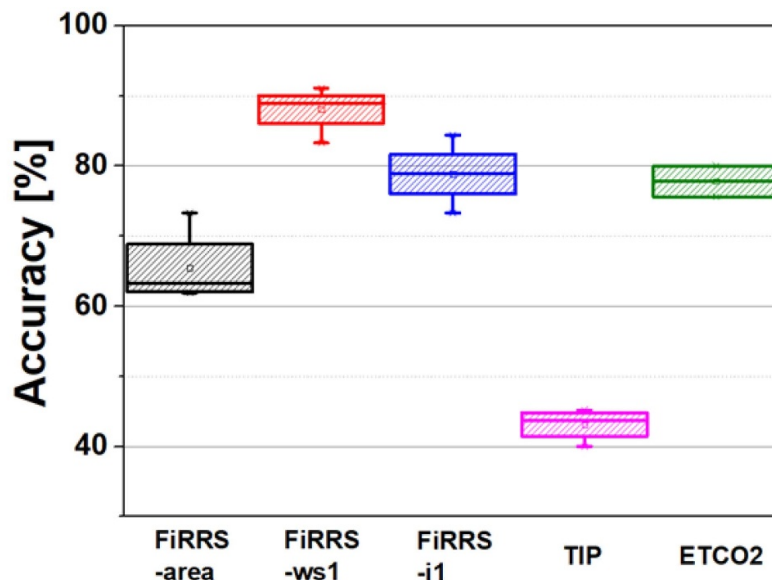
3.3. Part 2 study: analysis of low tidal volume breathing

Figure 7 shows the example of continuous data of three measurements: wavelength shift of FBG1, intensity change of the peak of FBG1 and the area under the spectrum for the three minutes of respiration recording when a participant was breathing using an anaesthetic mask (figure 3). The main

aim of part 2 was to demonstrate statistically the sensitivity of our device in distinguishing between normal and low tidal volumes of respiration. As discussed in section 3.1, the area under the spectrum data has lower intensity and so a smoothing filter (sgolayfilt—Savitzky-Golay finite impulse response (FIR) smoothing filter of polynomial order 4 and frame length 17) is applied to aid visualisation (green line, figure 7).



(a)



(b)

Figure 6. (a) Accuracy (%) of the correct measured RR values for every oxygen delivery device (CO₂ mask, nasal cannula and non-rebreathe trauma mask). Accuracy was calculated for every parameter of the FiRRS system (area under the spectrum, ws1 = wavelength shift FBG1, i1 = intensity change FBG1) and commercial devices (TIP and EtCO₂), all as a percentage when compared to the total correct values of manual counting (MC). (b) Combined accuracy data distribution in a box and whisker plot for all three parameters of the FiRRS system and the two commercial devices.

The participant was asked to reduce breathing tidal volume at the start of the second minute (following a pneumotacograph’s display) and to start to breathe normally again at the third minute of recording. As part of the post-processing analysis of part 2, the maximum difference between peaks and troughs during each period was measured for all participants (figure 8). 80% out of 15 participants produced a measurable signal response from both the wavelength shift and intensity of FBG1 and 53% participants for the area under the curve response.

Figure 8 present a comparison of the maximum absolute differences (peak to trough) measured before, during and after low tidal volume breathing for each participant that

presented a measurable response during the study. Figure 8(a) shows a whisker plot of the maximum differences for the wavelength shift of FBG1 measured before, during and after breathing at low tidal volume from the participants of part 2 of this study. Figure 8(b) presents the whisker plot of the maximum differences for the intensity change of FBG1 and figure 8(c) shows the whisker plot of the maximum differences for the area under the spectrum values measured from the participants.

All data acquired in part 2 of the study presented normal distribution around the mean following Kolmogorov–Smirnov tests (*p*-value > 0.05) on each, i.e. differences distribution

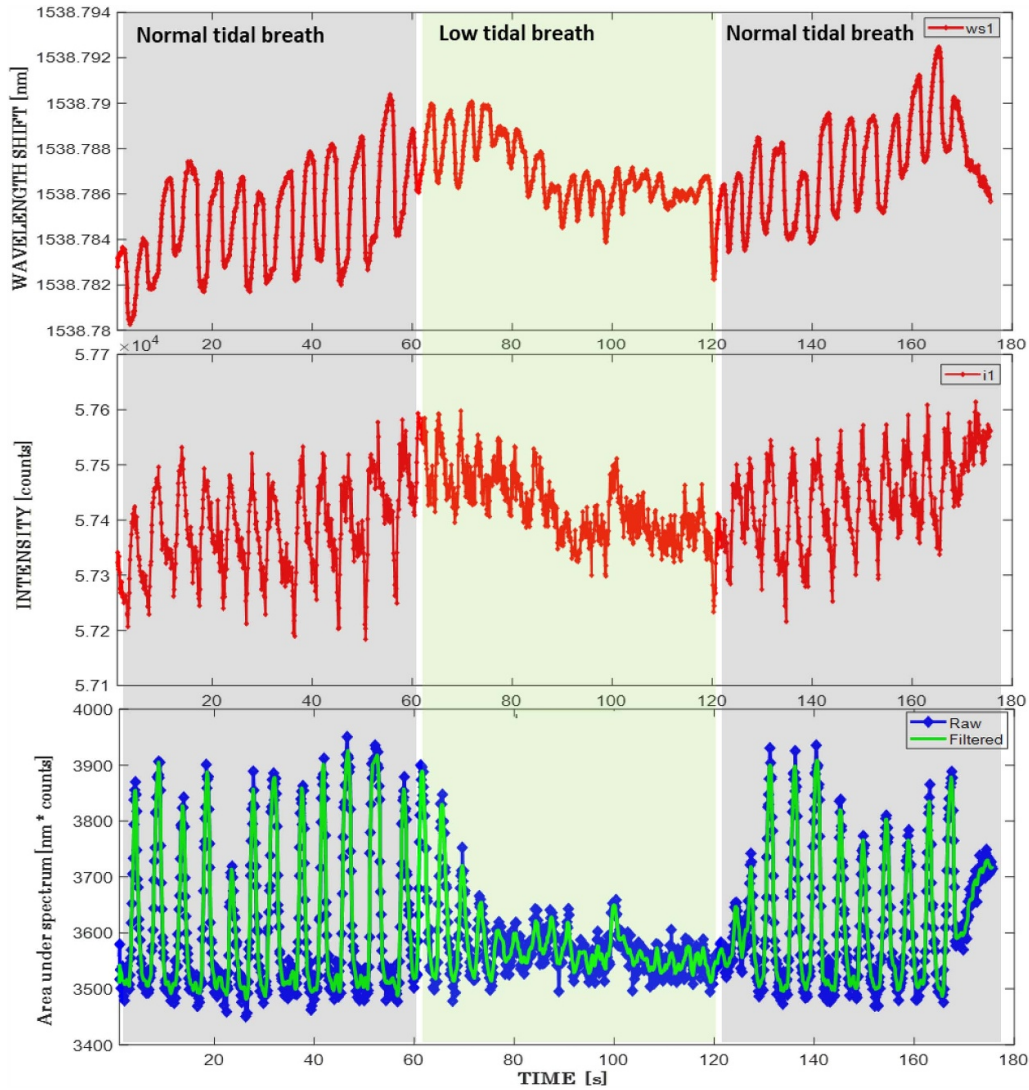


Figure 7. Three minutes recording of a participant wearing an anaesthetic mask (figure 3) before, during and after low tidal volume breathing following the protocol of part 2 of this study. Top and middle figure represents the wavelength shift and intensity change of the peak of FBG1 respectively. The lower figure is the change of area under the spectrum with filtered data shown in green.

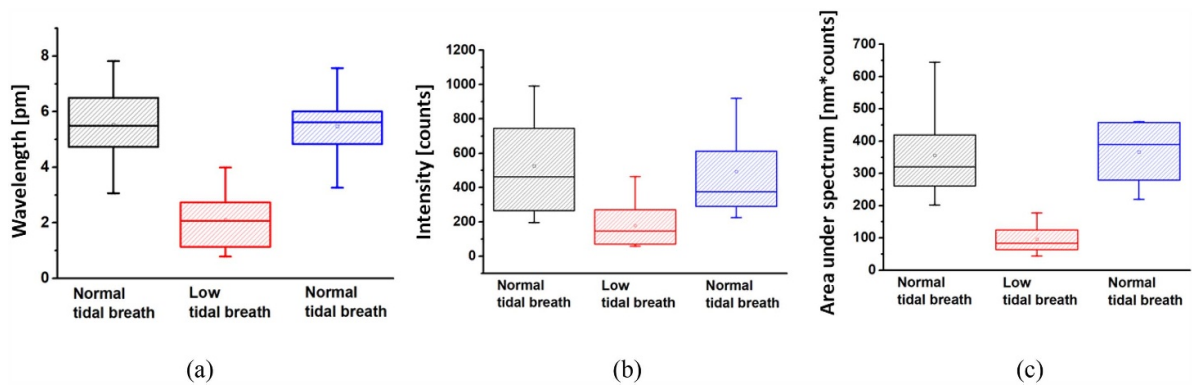


Figure 8. (a) Whisker plot of the maximum peak-to-trough of wavelength shift of FBG1 measured from the participants of part 2 of the study ($N = 12$). (b) Whisker plot of the maximum differences for the intensity change of FBG1 measured from the participants of part 2 of the study ($N = 11$). (c) Whisker plot of the maximum differences for the area values measured during part 2 of the study and with participants that presented measurable response ($N = 8$).

gathered from wavelength shift of FBG1 (figure 8(a)), intensity of FBG1 (figure 8(b)) and area values (figure 8(c)) across the participants. In addition, Student's *t*-tests demonstrated that there is no significant difference (p -value > 0.05) between the first and third minute recorded (normal tidal volumes) for all measurements shown in figure 8. Similarly, *t*-tests demonstrated that there is a significant difference (p -value < 0.05) between the first (normal tidal volume) and second (low tidal volume) measured for all measurements shown in figure 8.

4. Discussion

In part 1 of this volunteer study, the most accurate measurement of RR was through monitoring the wavelength shift of FBG1 (mean % accuracy = $88.1\% \pm 2.9\%$). The intensity change of FBG1 (mean % accuracy = $78.9\% \pm 3.9\%$) and EtCO₂ capnometry (mean % accuracy = $77.8\% \pm 2.2\%$) were similar and these were followed by the area under the spectrum (mean % accuracy = $65.4\% \pm 4.6\%$) and TIP (mean % accuracy = $43.1\% \pm 2.0\%$). In line with other studies, EtCO₂ capnometry along with manual counting are gold standards when compared to novel devices aimed to predict RR [13, 30, 31]. The improved accuracy of EtCO₂ capnometry when compared with TIP has also been reported [14].

The wavelength shift of FBG1 (ws_1) presented the highest accuracy due to the highly sensitive temperature response of the Bragg grating directly exposed to the breath temperature change near the tip of the encasing needle. The intensity change of FBG1 and the area under the spectrum are parameters that depend on the reflection change due to the hydrophilic properties of the PAH/SiO₂ NPs film deposited at the tip of the fibre. One would expect that the accuracy of the area and intensity parameters of FBG1 would be equal at first sight. However, the change of area under the spectra was affected by the amplitude of the overall reflection, for instance the area of the spectrum was limited between 1529 nm and 1581 nm (figure 4) and was typically $\sim 7\%$ of the maximum FBG amplitude. Thus, detection of variations for the area change are more affected by the noise floor of the system. This could be overcome by increasing the integration time of the spectrometer (fixed at 600 μs in this study) but at the expense of saturating the peak of the FBG signal. Alternatively, the properties of the film or FBG could be adjusted to change their relative reflectivity. The humidity sensing film [17] was fabricated with SiO₂ NPs without any further chemical dissolution in deionised water, therefore, the sensing film created with PAH/SiO₂ NPs tends to form more aggregates when using high SiO₂ NPs concentration. Using low SiO₂ NPs concentrations at 5 wt% [23] forms a more uniform film with a better controlled thickness over layer-by-layer. It should also be noted that the worst results for the area under the spectrum case were for volunteers P5, P6 and P7 (table 1) when there was 1 Hz total sampling rate for the spectrum data. Performance notably improved when the total sampling frequency was increased to 10 Hz.

It is well-known that TIP is prone to RR inaccuracies due to incorrect ECG electrode placement and motion artefacts due to chest wall movements different from respiration such as coughing or talking [14]. In addition, traditional TIP has been identified to have cardiac-derived artefacts that interfere with the RR measurements and, therefore, further developments have attempted to modify TIP by including adaptive filters and scaled Fourier linear combiners to remove the cardiac and bioimpedance interferences [32]. In this research work, the developed FiRRS system has demonstrated better accuracy than TIP when using the three oxygen delivery devices investigated, and a similar accuracy to EtCO₂ capnometry when using face masks.

Initial results from the FiRRS system are promising but improvements are still possible and will be explored in future work. These improvements will be particularly beneficial for the challenging respiration measurements at low tidal volume. As discussed, the relative intensity of the reflection from the tip and FBG1 is imbalanced. This could be addressed by reducing the reflectivity of the FBGs so that it is comparable to that from the tip. Low intensity could then be compensated by either increasing the integration of the spectrometer or increasing the intensity of the light source. Alternatively, if the FBGs are removed the integration times could be increased without detector saturation and the area under the spectrum could be used to obtain RR. This measurement is important because it represents performance that could be achieved with low cost instrumentation i.e. a single LED and photodetector compared to a more expensive FBG interrogation optoelectronic unit. The measured variability from all the parameters obtained with the FiRRS system was larger than the variability measured with the commercial devices (see whiskers of box plot, figure 6). This issue can be further refined through improvements of the FFT signal processing and the application of improved filtering to enhance the peak power over the noise floor.

As noted in the introduction, the commercially available respiR8 can perform poorly when operating at low expiratory flow rates and when water condensation is present on the sensor. In preliminary tests at low tidal volume (part 2) the system was demonstrated to be able to differentiate between low tidal volume and normal breathing. After further optimisation of the signal to noise ratio and signal processing of the system, tests will be conducted with more volunteers to explore the potential for measuring RR at low tidal volume. No obvious condensation effects were observed on the sensor or within the data, however, this should be explored with further testing in different environments within the clinic and community testing. As noted in previous work [17] condensation can be significantly reduced by embedding the sensor in a wool foam which prevents condensation. Different environments would also allow us to test the effect of ambient temperature of the mask. This is only a concern for identifying low tidal volume as for RR monitoring alone it is only important to monitor changes in the signal level and not absolute values. Ambient temperature is unlikely to cause a problem as the mask will have its own microenvironment with temperature close to that of the human body ($\sim 34.5^\circ\text{C}$) [33]. However, if

required, ambient temperature can be obtained from reference FBG2. Future work will also include real time data analysis and display and further miniaturisation of the opto-electronics to make a more portable device.

5. Conclusions

Using a descriptive statistical analysis, the FiRRS system developed in this research demonstrated 10% higher accuracy than a EtCO₂ capnometry device used in anaesthesia and these two monitors measured RR more accurately than TIP. A comparable accuracy in the measurement of RR was obtained between nasal cannula and the face masks tested when implementing the FiRRS system which allows measurement of RR after implementation of post-processing analysis of the light reflection spectra obtained. A second part of this study has demonstrated the feasible implementation of the FiRRS system developed in this work to differentiate between normal and low tidal volumes. This work targeted three RR values in part 1 of the study: 5 bpm, 12 bpm and 30 bpm. The rates 5 bpm and 30 bpm were conducted to test detection accuracy with the FiRRS system outside the normal range and only 12 bpm was chosen within the normal respiratory range. Our findings indicate that reflectance spectrometry techniques show similar accuracy to capnometry and may be more suitable with some oxygen delivery devices. Portable, inexpensive devices using these techniques could enable routine networked monitoring of respiratory function in vulnerable patients.

Acknowledgments

This work was supported by the Engineering and Physical Sciences Research Council (EPSRC) (Grant Nos. EP/N026985/1 and EP/R511730/1). Thanks to Dr Mark Faghy from the University of Derby (UK) for useful suggestions during the paper preparation.

ORCID iDs

C He  <https://orcid.org/0000-0002-4679-3160>
 S Korposh  <https://orcid.org/0000-0001-5179-6991>
 R Correia  <https://orcid.org/0000-0001-6405-5340>
 S P Morgan  <https://orcid.org/0000-0003-4069-3801>

References

- [1] Arozullah A M, Daley J, Henderson W G and Khuri S F 2000 Multifactorial risk index for predicting postoperative respiratory failure in men after major noncardiac surgery *Ann. Surg.* **232** 242–53
- [2] Dong Z, Xu X, Wang C, Cartledge S, Maddison R and Shariful Islam S M 2020 Association of overweight and obesity with obstructive sleep apnoea: a systematic review and meta-analysis *Obes. Med.* **17** 100185
- [3] Young T, Peppard P E and Gottlieb D J 2002 Epidemiology of obstructive sleep apnea: a population health perspective *Am. J. Respir. Crit. Care Med.* **165** 1217–39
- [4] Venn P J 2011 Obstructive sleep apnoea and anaesthesia *Anaesth. Intensive Care Med.* **12** 313–8
- [5] Liu H, Allen J, Chen D Z and Chen F 2019 Recent development of respiratory rate measurement technologies *Physiol. Meas.* **40** 07TR01
- [6] Meredith D J, Clifton D, Charlton P, Brooks J, Pugh C W and Tarassenko L 2011 Photoplethysmographic derivation of respiratory rate: a review of relevant physiology *J. Med. Eng. Technol.* **36** 1–7
- [7] Charlton P H, Bonnici T, Tarassenko L, Clifton D A, Beale R and Watkinson P J 2016 An assessment of algorithms to estimate respiratory rate from the electrocardiogram and photoplethysmogram *Physiol. Meas.* **37** 610–26
- [8] Yoon J-W, Noh Y-S, Kwon Y-S, Kim W-K and Yoon H-R 2014 Improvement of dynamic respiration monitoring through sensor fusion of accelerometer and gyro-sensor *J. Electr. Eng. Technol.* **9** 334–43
- [9] Bahmed F, Khatoun F and Reddy B R 2016 Relation between respiratory rate and heart rate comparative study *IJCAP* **3** 436–9
- [10] Sifuentes E, Cota-Ruiz J and Gonzalez-Landaeta R 2016 Respiratory rate detection by a time-based measurement system *Rev. Mex. Ing. Biomed.* **37** 91–99
- [11] Massaroni C, Venanzi C, Silvatti A P, Lo Presti D, Saccomandi P, Formica D, Giurazza F, Caponero M A and Schena E 2018 Smart textile for respiratory monitoring and thoraco-abdominal motion pattern evaluation *J. Biophoton.* **11** e201700263
- [12] Kano S, Dobashi Y and Fujii M 2018 Silica nanoparticle-based portable respiration sensor for analysis of respiration rate, pattern, and phase during exercise *Sensor Mater.* **2** 1–4
- [13] Niesters M, Mahajan R, Olofsen E, Boom M, Garcia Del Valle S, Aarts L and Dahan A 2012 Validation of a novel respiratory rate monitor based on exhaled humidity *Br. J. Anaesth.* **109** 981–9
- [14] Gaucher A, Frasca D, Mimos O and Debaene B 2012 Accuracy of respiratory rate monitoring by capnometry using the Capnomask[®] in extubated patients receiving supplemental oxygen *Br. J. Anaesth.* **108** 316–20
- [15] Wiklund L, Hök B, Ståhl K and Jordeby-Jönsson A 1994 Postanaesthesia monitoring revisited: frequency of true and false alarms from different monitoring devices *J. Clin. Anesth.* **6** 182–8
- [16] Sesay M, Tazuin-Fin P, Verdonck O, Svartz L and Maurette P 2008 Clinical evaluation of the CapnomaskTM in the supine vs. prone position during monitored anaesthesia care *Eur. J. Anaesthesiol.* **25** 769–71
- [17] Hernandez F U, Morgan S P, Hayes-Gill B R, Harvey D, Kinnear W, Norris A, Evans D, Hardman J G and Korposh S 2016 Characterization and use of a fiber optic sensor based on PAH/SiO₂ film for humidity sensing in ventilator care equipment *IEEE Trans. Biomed. Eng.* **63** 1985–92
- [18] Correia R, James S, Lee S-W, Morgan S P and Korposh S 2018 Biomedical application of optical fibre sensors *J. Opt.* **20** 073003
- [19] Kolpakov S A, Gordon N T, Mou C and Zhou K 2014 Toward a new generation of photonic humidity sensors *Sensors* **14** 3986–4013
- [20] Korposh S, James S, Tatam R P and Lee S-W 2012 Optical fibre long-period gratings functionalised with nano-assembled thin films: approaches to chemical sensing *Current Trends in Short- and Long-period Gratings*, ed Cuadrado-Laborde C (Rijeka: InTech) pp 63–86
- [21] Korposh S, Wang T, James S, Tatam R and Lee S-W 2012 Pronounced aromatic carboxylic acid detection using a layer-by-layer mesoporous coating on optical fibre long period grating *Sensors Actuators B* **173** 300–9

- [22] Hernandez F U, Correia R, Morgan S P, Hayes-Gill B R, Evans D, Sinha R, Norris A, Harvey D, Hardman J G and Korposh S 2016 Simultaneous temperature and humidity measurements in a mechanical ventilator using an optical fibre sensor *Sixth European Workshop on Optical Fibre Sensors (EWOFS'2016)* (Limerick, Ireland) (<https://doi.org/10.1117/12.2236850>)
- [23] He C, Korposh S, Hernandez F U, Liu L, Correia R, Hayes-Gill B R and Morgan S P 2020 Real-time humidity measurement during sports activity using optical fibre sensing *Sensors* **20** 1904
- [24] Dockney M L, James S W and Tatam R P 1996 Fibre Bragg gratings fabricated using a wavelength tuneable laser source and a phase mask based interferometer *Meas. Sci. Technol.* **7** 445–8
- [25] Massaroni C, Caponero M A, D'Amato R, Lo Presti D and Schena E 2017 Fiber Bragg grating measuring system for simultaneous monitoring of temperature and humidity in mechanical ventilation *Sensors* **17** S17040749
- [26] Kashyap R 2010 *Fiber Bragg Gratings* (San Diego, CA: Academic Press Elsevier)
- [27] Santos J S, Raimundo I M Jr, Cordeiro C M, Biazoli C R, Gouveia C A and Jorge P A 2014 Characterisation of a Nafion film by optical fibre Fabry-Perot interferometry for humidity sensing *Sensors Actuators B* **196** 99–105
- [28] World Medical Association 2013 Medical association declaration of Helsinki: ethical principles for medical research involving human subjects *JAMA* **310** 2191–4
- [29] O'Driscoll B R, Howard L S, Earis J and Mak V 2017 British thoracic society guideline for oxygen use in adults in healthcare and emergency settings *BMJ Open Respir. Res.* **4** e000170
- [30] van Loon K, Peelen L M, van de Vlasakker E C, Kalkman C J, van Wolfswinkel L and van Zaane B 2018 Accuracy of remote continuous respiratory rate monitoring technologies intended for low care clinical settings: a prospective observational study *Can. J. Anesth.* **65** 1324–32
- [31] Fukada T, Iwakiri H, Nomura M and Ozaki M 2015 Clinical evaluation of acoustic respiration rate monitoring compared with conventional systems in the postanaesthesia care unit *Eur. J. Anaesthesiol.* **32** 58–68
- [32] Yasuda Y, Umezu A, Horihata S, Yamamoto K, Miki R and Koike S 2005 Modified thoracic impedance plethysmography to monitor sleep apnea syndromes *Sleep Med.* **6** 215–24
- [33] Mack Cowan J, Burris J M, Hughes J R and Cunningham M P 2010 The relationship of normal body temperature, end-expired breath temperature, and BAC/BrAC ratio in 98 physically fit human test subjects *J. Anal. Toxicol.* **34** 238–42